Inorganic Chemistry

Article

pubs.acs.org/IC

Proton Conduction Study on Water Confined in Channel or Layer Networks of $La^{III}M^{III}(ox)_3 \cdot 10H_2O$ (M = Cr, Co, Ru, La)

Hisashi Ōkawa,[*,‡,§] Masaaki Sadakiyo,[†,∥] Kazuya Otsubo,[†,§] Ko Yoneda,[‡,⊥] Teppei Yamada,[†,⊗] Masaaki Ohba,[‡,§] and Hiroshi Kitagawa[*,†,§]

[†]Division of Chemistry, Graduate School of Science, Kyoto University, Kitashirakawa-Oiwakecho, Sakyo-ku, Kyoto 606-8502, Japan

[‡]Department of Chemistry, Faculty of Science, Kyushu University, Hakozaki 6-10-1, Higashi-ku, Fukuoka 812-8581, Japan

[§]Core Research for Evolutional Science and Technology, Japan Science and Technology Agency, Gobancho 7, Chiyoda-ku, Tokyo 102-0076, Japan

Supporting Information

ABSTRACT: Proton conduction of the $La^{III}M^{III}$ compounds, $LaM(ox)_3 \cdot 10H_2O$ (abbreviated to **LaM**; M = Cr, Co, Ru, La; ox^{2-} = oxalate) is studied in view of their networks. **LaCr** and **LaCo** have a ladder structure, and the ladders are woven to form a channel network. **LaRu** and **LaLa** have a honeycomb sheet structure, and the sheets are combined to form a layer network. The occurrence of these structures is explained by the rigidness versus flexibility of $[M(ox)_3]^{3-}$ in the framework with large La^{III}. The channel networks of **LaCr** and **LaCo** show a remarkably high proton conductivity, in the range from 1×10^{-6} to 1×10^{-5} S cm^{-1} over 40−95% relative humidity (RH) at 298 K, whereas the layer networks of **LaCr** and **LaCo** show a lower proton conductivity, $\sim 3 \times 10^{-8}$ S cm^{-1} (40−95% RH, 298 K). Activation energy measurements demonstrate that the channels filled with water molecules serve as efficient pathways for proton transport. **LaCo** was gradually converted to $La^{III}Co^{II}(ox)_{2.5} \cdot 4H_2O$, which had no channel structure and exhibited a low proton conductivity of less than 1×10^{-10} S cm^{-1}. The conduction−network correlation of $LaCo(ox)_{2.5} \cdot 4H_2O$ is reported.

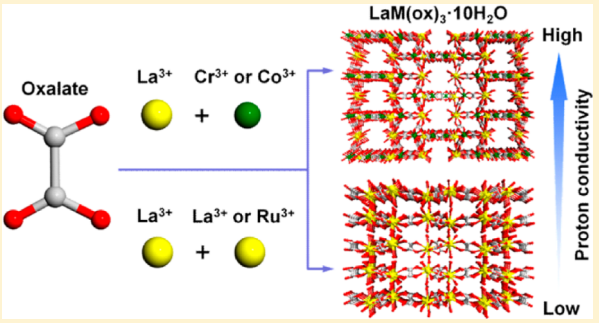

INTRODUCTION

Exploration and production of new proton-conductive materials have become important because of the materials' potential as components in solid-state electrochemical devices.[1−5] Naturally occurring materials such as $SrZrO_3$ and $CsHSO_4$ have been widely explored in proton conduction,[4a] and organic membranes represented by Nafion were produced as synthetic proton-conductive materials.[6−11] Recently, attention has been devoted to metal−organic framework (MOF) compounds because of the ease of deliberate design of ionic conduction pathways in their frameworks.[12−21] In particular, the molecularity and the crystallinity of MOFs enable us to understand proton conduction mechanisms on fundamental grounds. The bimetallic MOF compounds, $(A)[M_a^{II}M_b^{III}(ox)_3]$, first developed as molecular magnets,[22] have the advantage of producing proton-conductive materials by adopting hydrophilic cationic ions. In the compounds of $\{NH(CH_2CH_2CH_2OH)_3\}^+$ or $\{NR_3(CH_2COOH)\}^+$,[19] the hydrophilic ions residing between the bimetallic sheets serve as proton mediators or proton carriers and allow high proton conductivities of 1×10^{-4} S cm^{-1} at 75% relative humidity (RH) in $\{NH(CH_2CH_2CH_2OH)_3\}[MnCr(ox)_3] \cdot 2H_2O$ and 0.8×10^{-4} S cm^{-1} at 65% RH in $\{NMe_3(CH_2COOH)\}[FeCr(ox)_3] \cdot 3H_2O$. One weakness of these compounds is the instability to humidity inherent in the hydrophilic ions. To avoid this problem, we consider analogous compounds of the $M_a^{III}M_b^{III}(ox)_3$ type. Three families of this type have been reported: $LnCr(ox)_3 \cdot nH_2O$ (Ln = La, Nd; n = 10, 8) with a ladder structure,[23,24] $LnLn(ox)_3 \cdot nH_2O$ (Ln = La, Yb; n = 10, 5) with a honeycomb sheet structure,[25−28] and $LnCo(ox)_3 \cdot nH_2O$ (Ln = La or Pr; n = 10 or 8) with an unidentified structure.[29,30] Although they have no particular proton carriers in their frameworks, they have many water molecules, which may be responsible for proton conduction. In this work, we focus on the $La^{III}M^{III}$ compounds, $LaM(ox)_3 \cdot 10H_2O$ (abbreviated to **LaM**; M = Cr, Co, Ru, La), because LnM compounds of heavier lanthanide ions generally crystallize in lower hydrates. The proton conduction of the **LaM** was studied in view of their hydrogen-bonding networks. During this work, **LaCo** was found to be gradually converted into a $La^{III}Co^{II}$ compound, $LaCo(ox)_{2.5} \cdot 4H_2O$. The conduction−network characteristics of $LaCo(ox)_{2.5} \cdot 4H_2O$ were studied.

Received: May 28, 2015

DOI: 10.1021/acs.inorgchem.5b01176
Inorg. Chem. XXXX, XXX, XXX−XXX

EXPERIMENTAL SECTION

$K_3[Co(ox)_3]\cdot 3H_2O$, $K_3[Cr(ox)_3]\cdot 3H_2O$ and $K_3[Ru(ox)_3]\cdot 3H_2O$ were prepared using published methods.[31,32] Other chemicals were of reagent grade and were used as commercially purchased.

Preparation of $LaM(ox)_3\cdot 10H_2O$. *$LaCr(ox)_3\cdot 10H_2O$ (**LaCr**).* This was prepared by the reaction of $K_3[Cr(ox)_3]\cdot 3H_2O$ (245 mg) and $La(NO_3)_3\cdot 6H_2O$ (220 mg) in water (30 cm^3).[24] The hyacinth-colored crystalline solid was separated and dried over silica gel. Anal. Calcd (%) for $C_6H_{20}O_{22}CrLa$: C, 11.35; H, 3.17; Cr, 8.19; La, 21.87%. Found: C, 11.34; H, 3.11; Cr, 7.78; La, 22.10%. Fourier transform infrared (FT-IR): 1648 and 1435 cm^{-1}. UV−vis on powder sample: 17 500 and 24 100 cm^{-1}. μ_{eff}: 3.91 μ_B at 300 K.

*$LaCo(ox)_3\cdot 10H_2O$ (**LaCo**).* This was prepared by a modification of the literature method.[31] A solution of $La(NO_3)_3\cdot 6H_2O$ (220 mg) in water (10 cm^3) was added dropwise to a solution of $K_3[Co(ox)_3]\cdot 3H_2O$ (250 mg) in water (20 cm^3), and the mixture was stirred at ambient temperature for 30 min. Bright green crystals were collected, washed with water, and dried in the open air. Anal. Calcd (%) for $C_6H_{20}O_{22}CoLa$: C, 11.22; H, 3.14; Co, 9.18; La, 21.63%. Found: C, 11.17; H, 2.86; Co, 8.95; La, 22.01%. FT-IR: 1645 and 1438 cm^{-1}. UV−vis on powder sample: 15 500 and 22 600 cm^{-1}.

*$LaRu(ox)_3\cdot 10H_2O$ (**LaRu**).* A solution of $La(NO_3)_3\cdot 6H_2O$ (215 mg) in water (10 cm^3) was added dropwise to a stirred solution of $K_3[Ru(ox)_3]\cdot 3H_2O$ (282 mg) in water (15 cm^3). The resulting olive-green microcrystals were separated, washed with water, and dried in the open air. Anal. Calcd (%) for $C_6H_{20}O_{22}LaRu$: C, 10.53; H, 2.95; La, 20.30; Ru, 14.77%. Found: C, 10.48; H, 2.68; La, 20.61; Ru, 14.48%. FT-IR: 1612 and 1310 cm^{-1}. UV−vis on powder sample: 16 500, 23 300, and 28 200 cm^{-1}. μ_{eff}: 2.03 μ_B at 300 K.

*$La_2(ox)_3\cdot 10H_2O$ (**LaLa**).* This was prepared by the reaction of $La(NO_3)_3\cdot 6H_2O$ (215 mg) and $(NH_4)_2(ox)\cdot H_2O$ (215 mg) in water (30 cm^3).[33] Colorless microcrystals were separated, washed with water, and dried in air. Anal. Calcd (%) for $C_6H_{20}O_{22}La_2$: C, 9.98; H, 2.79; La, 38.48%. Found: C, 9.93; H, 2.82; La, 38.17%. FT-IR: 1609 and 1315 cm^{-1}.

Preparation of $LaCo(ox)_{2.5}\cdot 4H_2O$. $LaCo(ox)_3\cdot 10H_2O$ was heated at 100 °C under vacuum for 2 h to afford a pink powder. The weight loss by this treatment was 21.7%, which corresponded to the conversion to $LaCo(ox)_{2.5}\cdot 4H_2O$. Anal. Calcd (%) for $LaCo(ox)_{2.5}\cdot 4H_2O$ ($C_5H_8O_{14}CoLa$): C, 12.26; H, 1.65; Co, 12.03; La, 28.35%. Found: C, 12.21; H, 1.47; Co, 12.40; La, 28.16%. FT-IR: 1608 and 1312 cm^{-1}. UV−vis on powder sample: 8000 and 19 200 cm^{-1}. μ_{eff}: 4.97 μ_B at 300 K and 2.96 μ_B at 2.0 K.

Physical Measurements. X-ray powder diffraction (XRPD) measurements were performed using Bruker D8 ADVANCE (λ = 1.54059 Å; Cu Kα). Infrared spectra were recorded on a JASCO FT/IR-4200 FT-IR spectrophotometer equipped with ATR. Electronic spectra were measured by reflection on a pellet compacted with CaF_2 using a JASCO V-570 spectrophotometer. Thermogravimetric analyses were performed using a Bruker TG-DTA 2000SA at a heating rate of 5 K min^{-1} in a constant flow of N_2 gas. Water vapor adsorption/desorption isotherms were measured using BELSORP-max (MicrotracBEL Corp.) at 298 K. Samples were dehydrated at 60 °C under vacuum overnight. Proton conductivities were measured by the impedance method on sample pellets (~0.8 mm thickness × 2.5 mmϕ) prepared under a pressure of ~1.2 GPa. The impedance measurements were performed in the temperature range of 298−353 K by a conventional quasi-four-probe method using gold paste and gold wires (50 μmϕ), with a Solartron SI 1260 Impedance/Gain-Phase Analyzer and 1296 Dielectric Interface in the frequency range from 1 Hz to 1 MHz. Relative humidity was controlled using an Espec Corp. SH-221 incubator.

RESULTS AND DISCUSSION

Structures and Networks of LaM Compounds. The **LaM** compounds are classified into two networks: (1) **LaCr** and **LaCo** form a channel network made of ladders (Figure 1); and (2) **LaRu** and **LaLa** form a layer network made of honeycomb sheets (Figure 2). The crystal of **LaCr** has a coplanar ladder structure with the alternate array of Cr and La ions (Figure 1a).[24] The ladder chain is zigzag-shaped with Cr ions at the hollow sites and La ions at the projecting sites. The Cr has the $\{Cr(ox)_3\}$ surrounding in the usual D_3 symmetry,[34,35] and the La has a 10-coordinate $\{La(ox)_3(H_2O)_4\}$ surrounding. In the bulk, the ladders are woven to form a channel network filled with water molecules (Figure 1b). The channels including hydrogen-bonding networks run along the *b*-axis and also along the *c*-axis (Figure 1c). The arrangement and hydrogen bond distances between water in the channel are given in Figure S1 and Table S1. The water molecules form strong hydrogen bonds with the O···O distances ranging from 2.478 to 3.192 Å, affording the infinite network of hydrogen bond in the channel. Such infinite network of water molecules is one of the preferable systems for efficient proton transport through proton transfers between the molecules, called the Grotthuss mechanism.[36] **LaLa** has a honeycomb sheet structure with a nine-coordinate $\{La(ox)_3(H_2O)_3\}$ surrounding (Figure 2a).[27] In the bulk, the sheets are layered along the molecular *b*-axis to afford a layer network (Figure 2b). The honeycomb-shaped voids do not form large channels vertical to the layers because of offsets of the layers. The water molecules were included in the channel along the [011] direction (Figure 2c). In contrast to **LaCr**, these uncoordinated water molecules do not seem to form the infinite hydrogen bond network (Figure S2) as inferred from the low occupancies of the water molecules (occupancies: O(10) 50%, O(11) 50%, O(12) 50%, and O(13) 25%), even though there are short O···O distances between the oxygen sites (listed in Table S2). The hydrogen-bonding feature of

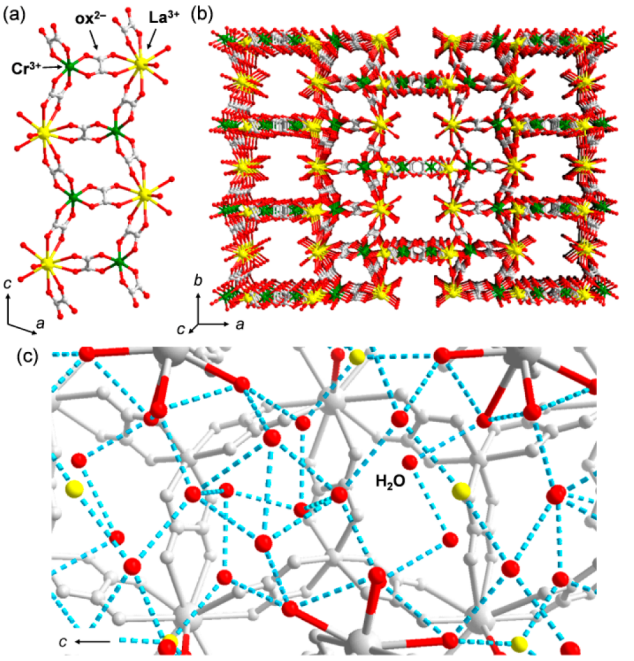

Figure 1. Representation of the crystal structure of **LaCr**. (a) The ladder structure and (b) one-dimensional channel with a $[LaCr(ox)_3(H_2O)_4]$ framework. The guest water molecules adsorbed in the channel are omitted. The yellow, green, gray, and red colors correspond to lanthanum, chromium, carbon, and oxygen atoms, respectively. (c) Hydrogen-bonding networks (blue dotted line) among the included water molecules (red). Yellow color corresponds to water molecules having 50% occupancy.

DOI: 10.1021/acs.inorgchem.5b01176
Inorg. Chem. XXXX, XXX, XXX−XXX

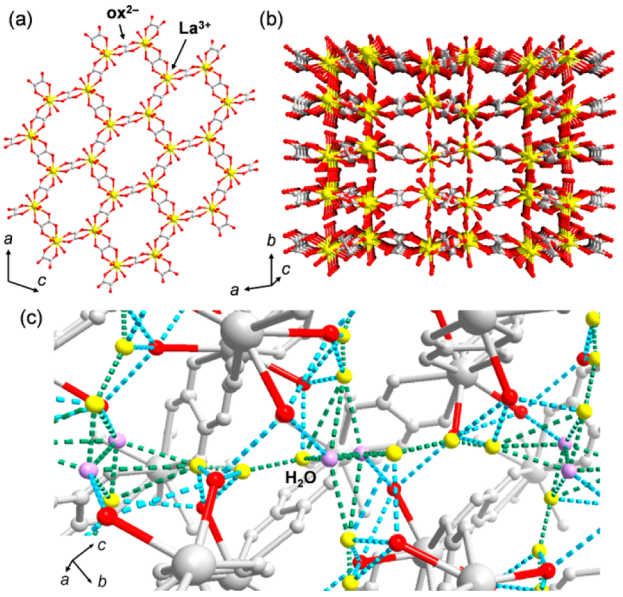

Figure 2. Representation of the crystal structure of **LaLa**. (a) The honeycomb layer structure and (b) a layered structure consisting of a $[LaLa(ox)_3(H_2O)_6]$ framework. The guest water molecules are omitted. The yellow, gray, and red colors correspond to lanthanum, carbon, and oxygen atoms, respectively. (c) Hydrogen-bonding networks (blue dotted line) among the included water molecules (red). Yellow and purple correspond to water molecules having 50 and 25% occupancy, respectively. Green dotted lines show hydrogen bonds between the disordered water molecules, which might not form in the actual case.

LaCr and **LaLa** is recalled later in the discussion of proton conduction.

To confirm the structures of the samples, we performed XRPD measurements for **LaCo**, **LaCr**, **LaRu**, and **LaLa** (Figure 3). The pattern for **LaCr** provides good agreement with the simulated pattern for the ladder framework of $LaCr(ox)_3 \cdot 10H_2O$.[24] **LaCo** shows almost the same pattern, showing that **LaCo** also has the same ladder structure. In contrast, **LaLa** and **LaRu** show patterns that are almost the same as the simulated pattern for the honeycomb-shaped framework of $LaLa(ox)_3 \cdot 10H_2O$.[27] Note that these samples do not show additional peaks compared with the simulation pattern, confirming the high purity of the samples. These results clearly show that the **LaM** compounds can be classified into two groups: (1) **LaCr** and **LaCo** with the channel network made from the ladders and (2) **LaRu** and **LaLa** with the layer network made from the honeycomb sheets. The honeycomb sheet structure is common for $(A)[M_a^{II}M_b^{III}(ox)_3]$,[37−41] but the ladder structure is limited to **LaCr** and **LaCo** as far as we know.

Why do these structures arise in **LaM**? The ionic radius of the M^{III} has no substantial effect upon the structures except for an alternation in the La···M separation. The distinction between **LaCr** or **LaCo** and **LaRu** is particularly notable because $(A)[M^{II}Cr^{III}(ox)_3]$,[37] $(A)[M^{II}Co^{III}(ox)_3]$,[42] and $(A)[M^{II}Ru^{III}(ox)_3]$[43] have similar honeycomb sheet structures. We suppose that the honeycomb sheet structure is preferred for $M_a^{III}M_b^{III}(ox)_3$, but a confusion occurs in the $La^{III}M^{III}$ compounds owing to the involvement of the large La^{III}. We note that the ladder structure is associated with the 4f/3d combination, while the sheet structure is associated with the 4f/4d combination. Thus, the transition M^{III} seems to play a role, in association with La^{III}, in determining the preferred structure.

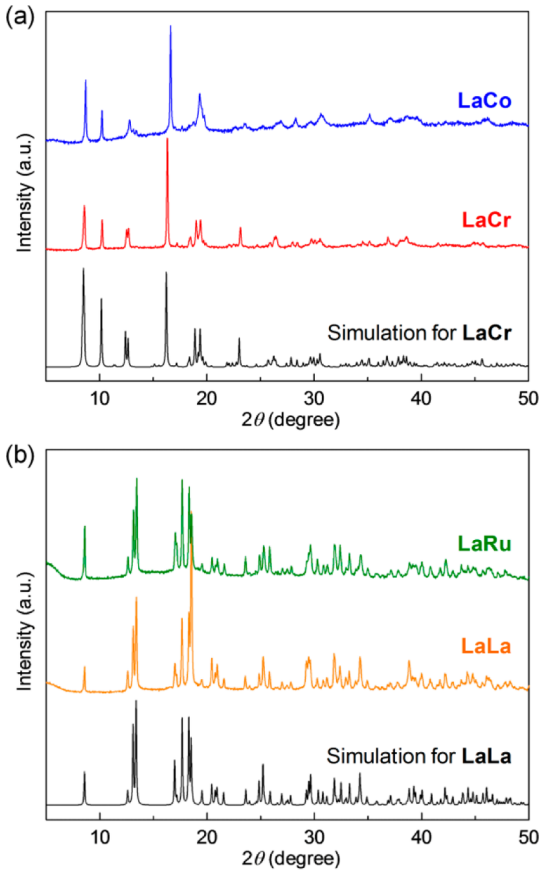

Figure 3. XRPD patterns of (a) **LaCo**, **LaCr**, (b) **LaRu**, and **LaLa**. Simulation patterns for **LaCr**[24] and **LaLa**[27] are shown in black.

Apart from the role of the M^{III}, we begin with the coordination characteristics of La^{III} in **LaLa**. It has a rugged honeycomb sheet with alternately upward and downward displacements of La atoms from the least-squares plane (Figure 4, left). This is

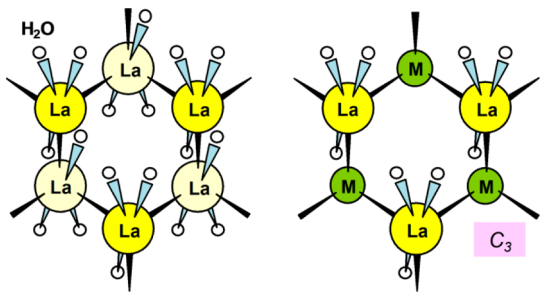

Figure 4. (left) The rugged honeycomb sheet of **LaLa** with alternately upward and downward displacement of La atoms and (right) the honeycomb sheet of **LaM** with C_3 symmetric $\{M(ox)_3\}$.

associated with the large and asymmetrical $\{La(ox)_3(H_2O)_3\}$ having one water molecule on one side and two water molecules on the other. The honeycomb sheet of **LaM** with a transition M^{III} ion is depicted by replacing the $\{La(ox)_3(H_2O)_3\}$ parts in the alternate positions with the $\{M(ox)_3\}$ parts (Figure 4, right). Because the rugged sheet also occurs with $LaM(ox)_3 \cdot 10H_2O$, the $\{M(ox)_3\}$ part must have a distorted geometry in near-C_3 symmetry. Because $[Cr(ox)_3]^{3-}$ and $[Co(ox)_3]^{3-}$ persist in maintaining the D_3 symmetric geometry, **LaCr** and **LaCo** cannot have the sheet

DOI: 10.1021/acs.inorgchem.5b01176
Inorg. Chem. XXXX, XXX, XXX−XXX

structure, but must assume the ladder structure. It is generally believed that $[Ru(ox)_3]^{3-}$ assumes a D_3 symmetric geometry, but $K_3[Ru(ox)_3]\cdot 4.5H_2O$[32] shows a remarkable distortion from D_3 symmetry, along with a deformation in oxalato-Ru chelate rings. This is taken as an indication that $[Ru(ox)_3]^{3-}$ is quite flexible so that it can adapt to the C_3 symmetric sites of the sheet. In summary, the preferred structure of **LaM** depends upon the rigidity versus flexibility of $[M(ox)_3]^{3-}$ in its association with large La^{III}.

The ladder structure and the honeycomb structure are distinguished by IR spectroscopy. **LaCr** and **LaCo** (ladder structure) have the antisymmetric CO stretching band of the oxalate bridge, ν_{as}(CO), at ~1647 cm^{-1} and the symmetric CO stretching band, ν_s(CO), at ~1435 cm^{-1}, whereas $LaRu(ox)_3\cdot 10H_2O$ and $LaLa(ox)_3\cdot 10H_2O$ (layer structure) have the ν_{as}(CO) band at ~1610 cm^{-1} and the ν_s(CO) band at ~1315 cm^{-1} (exact numerical data are given in the Experimental Section). The distinct IR patterns are correlated to the unit structures, that is, the tetragonal $La_2M_2(ox)_4$ unit of the ladder and the hexagonal (honeycomb) $La_3M_3(ox)_6$ unit in the honeycomb sheet. The criterion of the unit structures by IR spectroscopy shall be recalled later in the identification of the $La^{III}Co^{II}$ compound, $LaCo(ox)_{2.5}\cdot 4H_2O$, derived from **LaCo**.

The channel network made of the ladders and the layer network made of the honeycomb sheets are differentiated by thermogravimetry (Figure 5). **LaCr** and **LaCo** (channel networks) show a gradual weight decrease to reach a near plateau at 200−350 °C. The weight loss at 350 °C is ~28% for both compounds. This corresponds to the dehydration to anhydrous $LaCr(ox)_3$ (calcd H_2O weight loss: 28.3%) and $LaCo(ox)_3$ (28.1%). **LaRu** and **LaLa** (layer networks) exhibit stepwise dehydration processes. In **LaRu**, three water molecules are released at ~100 °C, followed by the release of three water molecules at ~130 °C, two water molecules at ~270 °C, and two water molecules at ~370 °C. In **LaLa**, five water molecules are released at ~140 °C, followed by the release of three water molecules at ~300 °C and two water molecules at ~350 °C. Anhydrous $LaRu(ox)_3$ and $LaLa(ox)_3$ are not stabilized. Instead, $LaRu(ox)_3\cdot 4H_2O$ is stabilized at 130−210 °C, while $LaLa(ox)_3\cdot 5H_2O$ is stabilized at 140−220 °C. In a previous thermal study of **LaLa**, no intermediate hydrates were detected.[33]

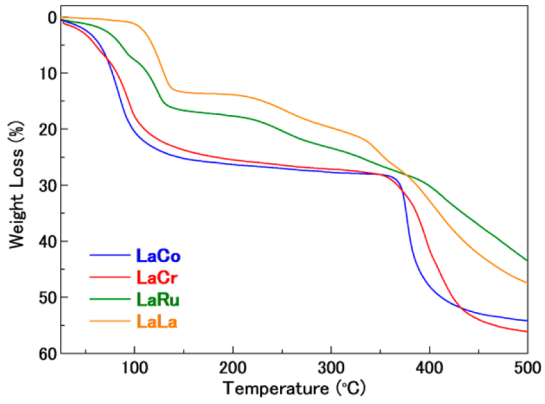

Figure 5. Thermogravimetric curves of **LaM**.

Proton Conduction of LaM. The LaM compounds are stable to moisture, allowing conduction measurements up to 95% RH. Proton conductivities were measured at 298 K using the alternating current impedance method on pellet samples. The $\log(\sigma/S\ cm^{-1})$ versus RH profiles are shown in Figure 6. **LaCr** and **LaCo** with their channel networks with infinite hydrogen-bonding networks display a remarkably high proton conductivity in the range from 1×10^{-6} to 1×10^{-5} S cm^{-1} over 40−95% RH at 298 K, whereas **LaRu** and **LaLa** with their layer networks, which do not have infinite hydrogen-bonding networks, show two orders lower conductivity, ~3×10^{-8} S cm^{-1} (40−95% RH at 298 K). Note that **LaRu** and **LaLa** have the same layer network and show similar proton conductivity. This means that the Ru site of **LaRu** has the 10-coordinate $\{Ru(ox)_3(H_2O)_4\}$ surrounding like $\{La(ox)_3(H_2O)_4\}$ in **LaLa**. Therefore, Ru^{3+} can assume higher coordination under forced circumstances, while Ru^{3+}-complexes so far characterized have six-coordinate geometry. Because no proton carrier or acidic site exists, proton must be provided by the self-dissociation of water molecules coordinated to the metal centers or captured in the lattice. Coordinated water often enhances proton conductivity due to the Lewis acidity of the coordinating metal ions,[16a,44] but this contribution is not evident in the **LaM** compounds since the proton conduction is independent of the metal ion pair in each network. This result clearly shows that the difference in the proton-conducting pathways between them is directly related to the difference in the proton conductivity. The pink plot shows the conductivity of $LaCo(ox)_{2.5}\cdot 4H_2O$ (details are described below), having no channel structure, which is made from **LaCo**. This sample showed very low conductivity of less than 10^{-10} S cm^{-1}, suggesting that the large channel structure is critical to the high proton conduction in **LaCo**.

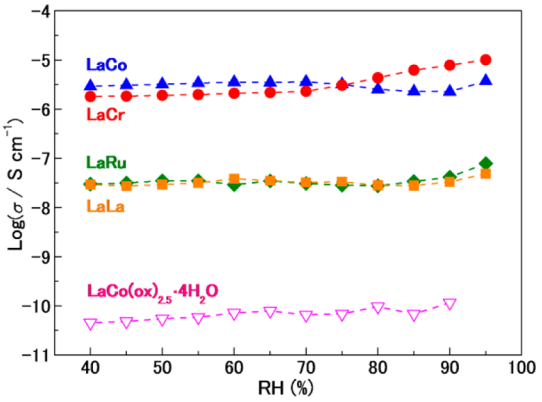

Figure 6. $\log(\sigma/S\ cm^{-1})$ vs RH profiles of **LaM** and $LaCo(ox)_{2.5}\cdot 4H_2O$ at 298 K.

Note that the proton conduction of the **LaM** compounds is practically independent of humidity, in contrast to most proton-conducting MOFs whose proton conduction is largely dependent on humidity.[13,14b,19] To inspect the humidity-independence of the proton conduction, we measured water vapor adsorption/desorption isotherms for **LaCr** at 298 K using samples thoroughly dehydrated at 60 °C under vacuum for several days (Figure 7). The water adsorption at 100% RH corresponds to ~10 molecules per the **LaCr** unit. In the desorption process, the adsorbed water is not substantially removed when RH is reduced to 40%. We think that few change in amount of water molecules caused such independence of conductivity from humidity. That is, the network of **LaCr** ($LaCr(ox)_3\cdot 10H_2O$) is fully saturated with water and is hardly dehydrated under ordinary humidity.

DOI: 10.1021/acs.inorgchem.5b01176
Inorg. Chem. XXXX, XXX, XXX−XXX

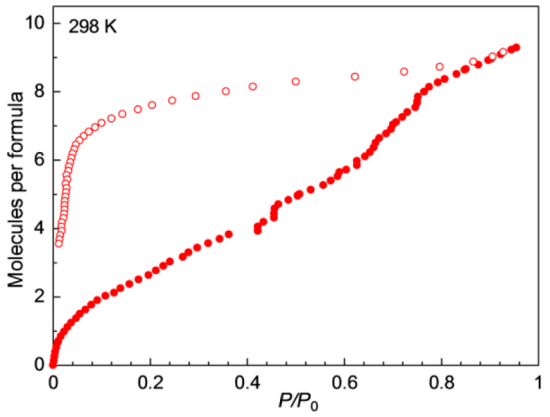

Figure 7. Water vapor adsorption/desorption isotherms of **LaCr** at 298 K.

To show explicitly the correlation between the network and the proton conduction, the activation energies were evaluated for **LaCr** (lager channels) and **LaRu** (smaller space). The Arrhenius plots of the $\log(\sigma T/\mathrm{S\ cm^{-1}\ K})$ values against the reciprocal of temperature are shown in Figure 8. **LaCr** shows a

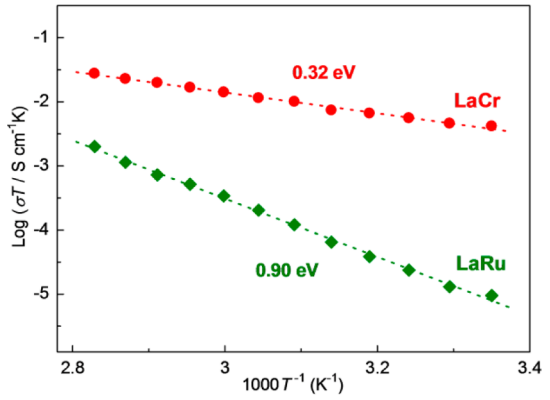

Figure 8. Arrhenius plots of proton conductivities in the range of 298−355 K under 95% RH: **LaCr** (red) and **LaRu** (green).

low activation energy of 0.32 eV, while **LaRu** shows a high activation energy of 0.90 eV. Obviously, the channel network of **LaCr** serves as efficient pathways for proton transport, whereas the layer network of **LaRu** serves moderately for proton transport. The proton conduction of two networks might be concerned with different mechanism. As mentioned above, the confined water molecules in the channel of **LaCr** form infinite hydrogen-bonding networks (Figure S1), which can be responsible for efficient proton transfer by Grotthuss mechanism.[36] However, the water molecules between the sheets of **LaLa** are rather loosely hydrogen-bonded (Figure S2) where proton transfer by Grotthuss mechanism must be less effective compared with the case of **LaCr**. We think that these structural features are consistent with the experimental values of the activation energies of **LaCr** (0.32 eV) and **LaRu** (0.90 eV), because good hydrated proton conductors with the Grotthuss mechanism normally show very low activation energy (less than ∼0.4 eV).[45] We think that the proton transport in **LaRu** includes some other process such as the direct diffusion of the disordered water molecules (vehicle mechanism[46]) in the channel.

Identification and Conduction−network Characteristics of $LaCo(ox)_{2.5}\cdot 4H_2O$. The green color of **LaCo** faded gradually to pink in a couple of weeks. The color change was accelerated on exposure to sunlight or at elevated temperatures. The resulting pink species exhibited a proton conductivity of less than 1×10^{-10} S cm^{-1}, lower by more than ∼5 orders of magnitude compared with the parent **LaCo** (Figure 6). Such color changes of trioxalatocobaltate(III) compounds have long been known and were explained by the transformation into a cobalt(II) species.[47−51] Usha reported thermal decomposition of **LaCo** to form pink-colored $La^{III}Co^{II}(ox)_{2.5}\cdot nH_2O$ in different hydrations, but the $La^{III}Co^{II}$ compound was not fully identified.[30] Because of our interest in conduction−network correlation, we performed the identification and characterization of the pink compound derived from **LaCo**.

For practical preparation, **LaCo** was heated at 100 °C in vacuum to obtain $LaCo(ox)_{2.5}\cdot 4H_2O$ with good reproducibility. The conversion is represented by the reaction $Co^{3+} + 0.5C_2O_4^{2-} = Co^{2+} + CO_2$. A sample prepared at 200 °C under ordinary pressure exhibited a characteristic IR band at 2340 cm^{-1} attributable to CO_2 captured in the lattice (Figure S3). This IR band disappeared on evacuation. The electronic spectrum of $LaCo(ox)_{2.5}\cdot 4H_2O$ has two visible bands at 8000 and 19 000 cm^{-1} (Figure S4), which are typical of the $\{Co^{II}O_6\}$ chromophore.[52] From the result of thermogravimetric analysis (Figure S5), the included four water molecules (calcd as 14.7% weight loss) of $LaCo(ox)_{2.5}\cdot 4H_2O$ were desorbed below 250 °C (14.6% weight loss), and the framework was decomposed at ∼380 °C as similar to **LaCo**. The $\chi_m T$ value at 300 K is 3.09 emu mol^{-1} K (or 4.97 μ_B), which decreases at lower temperatures to 1.10 emu mol^{-1} K (2.97 μ_B) at 2.0 K (Figure S6). The $\chi_m T$ versus T curve can be interpreted as the $^4T_1$ ground term of octahedral high-spin Co(II).[53] The curve displays a gradual downward departure from the theoretical curve at lower temperatures (1.77 emu mol^{-1} K (3.76 μ_B) is expected at 2 K), probably because of secondary effects such as zero-field splitting of $^4T_1$ or an intermolecular antiferromagnetic interaction. The spectral and magnetic results are consistent with $[Co^{II}(ox)_3]^{4-}$ existing in $LaCo(ox)_{2.5}\cdot 4H_2O$.

Most informative is the IR spectral feature with the $\nu_{as}(CO)$ band at 1608 cm^{-1} and the $\nu_s(CO)$ band at 1312 cm^{-1}. The IR pattern differs from that of parent $LaCo(ox)_3\cdot 10H_2O$ with the ladder structure ($\nu_{as}(CO)$ 1645 cm^{-1} and $\nu_s(CO)$ 1438 cm^{-1}), and is compared with the pattern of the **LaRu** and **LaLa** compounds of the honeycomb sheet ($\nu_{as}(CO) \approx 1610$ cm^{-1} and $\nu_s(CO) \approx 1315$ cm^{-1}). However, it is unlikely that the ladder of **LaCo** is transformed into the honeycomb sheet in $LaCo(ox)_{2.5}\cdot 4H_2O$ by the mild heating at 100 °C of a solid sample. Using the criterion mentioned above, we consider that $LaCo(ox)_{2.5}\cdot 4H_2O$ keeps the ladder structure but has a hexagonal $La_3Co_3(ox)_6$ unit instead of the tetragonal $La_2Co_2(ox)_4$ unit of **LaCo**. The transformation from the tetragonal-based ladder to the hexagonal-based ladder is schematically shown in Figure 9. The oxalate group in the alternate step is removed concomitantly with the reduction of Co^{III} to Co^{II}, followed by the migration of the Co^{II} to a hexagonal corner.

$LaCo(ox)_{2.5}\cdot 4H_2O$ displays no XRPD structures. The amorphous nature is understandable because any oxalate groups in the steps are involved in the conversion to cause a disorder in the hexagonal-based ladder and thence the destruction of the hydrogen-bonded network in the channel. We may conclude that $LaCo(ox)_{2.5}\cdot 4H_2O$ displays a low proton

DOI: 10.1021/acs.inorgchem.5b01176
Inorg. Chem. XXXX, XXX, XXX−XXX

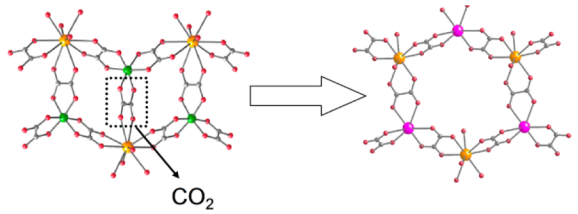

Figure 9. Schematic representation of the transformation of the square-based ladder to the hexagonal-based ladder (green: Co^{3+}, pink: Co^{2+}, yellow: La^{3+}).

conduction relative to parent **LaCo** because of a collapse of the pathways for proton transport.

CONCLUSION

The **LaM** are classified into two networks. **LaCr** and **LaCo** have the ladder structure, and the ladders are woven to form a channel network filled with water molecules. **LaRu** and **LaLa** have the honeycomb sheet structure, and the sheets are connected through hydrogen bonds to form a layer network. The occurrence of the ladder structure and the honeycomb structure in $LaM(ox)_3 \cdot 10H_2O$ (M = Cr, Co, Ru) is explained by the rigidness versus flexibility of $[M(ox)_3]^{3-}$ in their association with the large La^{III}. **LaCr** and **LaCo** with the channel network show very high proton conductivity in the range from 1×10^{-6} to 1×10^{-5} S cm^{-1} under 40−95% RH and at room temperature, even though there are no particular proton carriers in the framework. **LaRu** and **LaLa** with the layer network show moderate conductivity of $\sim 3 \times 10^{-8}$ S cm^{-1}. Together with activation energy studies, it is revealed that the channels filled with water serve as efficient pathways for proton transport. Pink-colored $LaCo(ox)_{2.5} \cdot 4H_2O$ derived from **LaCo** has a hexagonal-based ladder structure. It displays low proton conduction of less than 1×10^{-10} S cm^{-1}, because of a collapse of the pathways for proton transport. This work demonstrates that high proton conduction is achieved by a hydrogen-bonded network of water when the network is well-designed in MOFs.

ASSOCIATED CONTENT

Supporting Information

The Supporting Information is available free of charge on the ACS Publications website at DOI: 10.1021/acs.inorgchem.5b01176.

Illustrations of hydrogen-bonding networks and included water molecules in **LaCr** and **LaLa**, tabulated hydrogen bond distances in **LaCr** and **LaLa**, adsorption isotherms, IR spectral evidence of CO_2 captured in the lattice of the $La^{III}Co^{II}$ sample, electronic spectra of $LaCo(ox)_{2.5} \cdot 4H_2O$ and **LaCo**, and χ_M versus T and $\chi_M T$ versus T curves of $LaCo(ox)_{2.5} \cdot 4H_2O$. (PDF)

X-ray crystallographic information of **LaCo**. (CIF)

X-ray crystallographic information of **LaLa**. (CIF)

AUTHOR INFORMATION

Corresponding Authors

*E-mail: kitagawa@kuchem.kyoto-u.ac.jp. (H.K.)

*E-mail: okawa134(a)ac.auone-net.jp. (H.O.)

Present Addresses

∥International Institute for Carbon-Neutral Energy Research (WPI-I2CNER), Kyushu University, Moto-oka 744, Nishi-ku, Fukuoka, 819−0395, Japan.

⊥Department of Chemistry and Applied Chemistry, Graduate School of Science and Engineering, Saga University, Honjo-machi 1, Saga 840−8502, Japan.

⊗Center for Molecular Systems (CMS), Department of Chemistry and Biochemistry, Graduate School of Engineering, Kyushu University, Moto-oka 744, Nishi-ku, Fukuoka, 819−0395, Japan.

Notes

The authors declare no competing financial interest.

ACKNOWLEDGMENTS

This work was partly supported by the Grants-in-Aid for the Global COE Program, "Science for Future Molecular Systems" from the Ministry of Education, Culture, Science, Sports and Technology of Japan. The authors thank Prof. M. Sakamoto of Yamagata Univ. for many valuable advices.

REFERENCES

(1) Colomban, P. *Chemistry of Solid State Chemistry 2. Proton Conductors;* Cambridge Univ. Press: Cambridge, U.K., 1992.

(2) Service, R. F. *Science* **2002**, *296*, 1222−1224.

(3) Winter, M.; Brodd, R. J. *Chem. Rev.* **2004**, *104*, 4245−4269.

(4) (a) Kreuer, K. D. *Chem. Mater.* **1996**, *8*, 610−641. (b) Kreuer, K. D. *Solid State Ionics* **1997**, *97*, 1−15.

(5) Haile, S. M.; Boysen, D. A.; Chisholm, C. R. I.; Merle, R. B. *Nature* **2001**, *410*, 910−913.

(6) Mauritz, K. A.; Moore, R. B. *Chem. Rev.* **2004**, *104*, 4535−4586.

(7) Sumner, J. J.; Creager, S. E.; Ma, J. J.; DesMarteau, D. D. *J. Electrochem. Soc.* **1998**, *145*, 107−110.

(8) Kreuer, K. D. *J. Membr. Sci.* **2001**, *185*, 29−39.

(9) Woudenberg, R. C.; Yavuzcetin, O.; Tuominen, M. T.; Coughlin, E. B. *Solid State Ionics* **2007**, *178*, 1135−1141.

(10) Li, G. H.; Lee, C. H.; Lee, Y. M.; Cho, C. G. *Solid State Ionics* **2006**, *177*, 1083−1090.

(11) Halla, J. D.; Mamak, M.; Williams, D. E.; Ozin, G. A. *Adv. Funct. Mater.* **2003**, *13*, 133−138.

(12) (a) Ramaswamy, P.; Wong, N. E.; Shimizu, G. K. H. *Chem. Soc. Rev.* **2014**, *43*, 5913−5932. (b) Yamada, T.; Otsubo, K.; Makiura, R.; Kitagawa, H. *Chem. Soc. Rev.* **2013**, *42*, 6655−6669. (c) Horike, S.; Umeyama, D.; Kitagawa, S. *Acc. Chem. Res.* **2013**, *46*, 2376−2384. (d) Yoon, M.; Suh, K.; Natarajan, S.; Kim, K. *Angew. Chem., Int. Ed.* **2013**, *52*, 2688−2700. (e) Akutsu-Sato, A.; Akutsu, H.; Turner, S. S.; Day, P.; Probert, M. R.; Howard, J. A. K.; Akutagawa, T.; Takeda, S.; Nakamura, T.; Mori, T. *Angew. Chem.* **2005**, *117*, 296−299.

(13) (a) Fujishima, M.; Kanda, S.; Mitani, T.; Kitagawa, H. *Synth. Met.* **2001**, *119*, 485−486. (b) Nagao, Y.; Ikeda, R.; Kanda, S.; Kubozono, Y.; Kitagawa, H. *Mol. Cryst. Liq. Cryst.* **2002**, *379*, 89−94. (c) Nagao, Y.; Fujishima, M.; Kanda, S.; Ikeda, R.; Kitagawa, H. *Synth. Met.* **2003**, *133−134*, 431−432. (d) Nagao, Y.; Ikeda, R.; Iijima, K.; Kubo, T.; Nakasuji, K.; Kitagawa, H. *Synth. Met.* **2003**, *135−136*, 283−284. (e) Nagao, Y.; Kubo, T.; Nakasuji, K.; Ikeda, R.; Kojima, T.; Kitagawa, H. *Synth. Met.* **2005**, *154*, 89−92. (f) Fujishima, M.; Enyo, M.; Kanda, S.; Ikeda, R.; Kitagawa, H. *Chem. Lett.* **2006**, *35*, 546−547.

(14) (a) Sadakiyo, M.; Yamada, T.; Kitagawa, H. *J. Am. Chem. Soc.* **2009**, *131*, 9906−9907. (b) Sadakiyo, M.; Yamada, T.; Honda, K.; Matsui, H.; Kitagawa, H. *J. Am. Chem. Soc.* **2014**, *136*, 7701−7707. (c) Sadakiyo, M.; Yamada, T.; Kitagawa, H. *J. Am. Chem. Soc.* **2014**, *136*, 13166−13169.

(15) Miyatsu, S.; Kofu; Nagoe, A.; Yamada, T.; Sadakiyo, M.; Yamada, T.; Kitagawa, H.; Tyagi, M.; Garcia Sakai, V.; Yamamuro, O. *Phys. Chem. Chem. Phys.* **2014**, *16*, 17295−17304.

(16) (a) Yamada, T.; Sadakiyo, M.; Kitagawa, H. *J. Am. Chem. Soc.* **2009**, *131*, 3144−3145. (b) Morikawa, S.; Yamada, T.; Kitagawa, H. *Chem. Lett.* **2009**, *38*, 654−655. (c) Yamada, T.; Morikawa, S.; Kitagawa, H. *Bull. Chem. Soc. Jpn.* **2010**, *83*, 42−48. (d) Kanaizuka, K.; Iwakiri, S.; Yamada, T.; Kitagawa, H. *Chem. Lett.* **2010**, *39*, 28−29.

DOI: 10.1021/acs.inorgchem.5b01176
Inorg. Chem. XXXX, XXX, XXX−XXX

(17) (a) Bureekaew, S.; Horike, S.; Higuchi, M.; Mizuno, M.; Kawamura, T.; Tanaka, D.; Yanai, N.; Kitagawa, S. *Nat. Mater.* **2009**, *8*, 831−836. (b) Umeyama, D.; Horike, S.; Inukai, M.; Hijikata, Y.; Kitagawa, S. *Angew. Chem., Int. Ed.* **2011**, *50*, 11706−11709. (c) Horike, S.; Umeyama, D.; Inukai, M.; Itakura, T.; Kitagawa, S. *J. Am. Chem. Soc.* **2012**, *134*, 7612−7615. (d) Umeyama, D.; Horike, S.; Inukai, M.; Itakura, T.; Kitagawa, S. *J. Am. Chem. Soc.* **2012**, *134*, 12780−12785.
(18) (a) Hurd, J. A.; Vaidhyanathan, R.; Thangadurai, V.; Ratcliffe, C. I.; Moudrakovski, I. L.; Shimizu, G. K. H. *Nat. Chem.* **2009**, *1*, 705−710. (b) Taylor, J. M.; Mah, R. K.; Moudrakovski, I. L.; Ratcliffe, C. I.; Vaidhyanathan, R.; Shimizu, G. K. H. *J. Am. Chem. Soc.* **2010**, *132*, 14055−14057.
(19) (a) Ōkawa, H.; Shigematsu, A.; Sadakiyo, M.; Miyagawa, T.; Yoneda, K.; Ohba, M.; Kitagawa, H. *J. Am. Chem. Soc.* **2009**, *131*, 13516−13522. (b) Sadakiyo, M.; Ōkawa, H.; Shigematsu, A.; Ohba, M.; Yamada, T.; Kitagawa, H. *J. Am. Chem. Soc.* **2012**, *134*, 5472−5475. (c) Ōkawa, H.; Sadakiyo, M.; Yamada, T.; Maesato, M.; Ohba, M.; Kitagawa, H. *J. Am. Chem. Soc.* **2013**, *135*, 2256−2262.
(20) Sadakiyo, M.; Kasai, H.; Kato, K.; Takata, M.; Yamauchi, M. *J. Am. Chem. Soc.* **2014**, *136*, 1702−1705.
(21) Wiers, B. M.; Foo, M.-L.; Balsara, N. P.; Long, J. R. *J. Am. Chem. Soc.* **2011**, *133*, 14522−14525.
(22) (a) Zhong, Z. J.; Matsumoto, N.; Ōkawa, H.; Kida, S. *Chem. Lett.* **1990**, 87−90. (b) Tamaki, H.; Zhong, Z. J.; Matsumoto, N.; Kida, S.; Koikawa, M.; Achiwa, N.; Hashimoto, Y.; Ōkawa, H. *J. Am. Chem. Soc.* **1992**, *114*, 6974−6979.
(23) Sakamoto, M.; Matsuki, K.; Ohsumi, R.; Nakayama, Y.; Sadaoka, Y.; Nakayama, S.; Matsumoto, N.; Ōkawa, H. *Nippon Seramikkusu Kyokai Gakujutsu Ronbunshi* **1992**, *100*, 1211−1215.
(24) Decurtins, S.; Gross, M.; Schmalle, H. W.; Ferlay, S. *Inorg. Chem.* **1998**, *37*, 2443−2449.
(25) Birnbaum, E. R. In *Gmelin Handbook of Inorganic Chemistry;* Moeller, T., Schleitzer, E., Eds.; Springer-Verlag: Berlin, Germany, 1984; Vol. *39* (D5), p 120 and references therein.
(26) Ollendorff, W.; Weigel, F. *Inorg. Nucl. Chem. Lett.* **1969**, *5*, 263−269.
(27) Michaelides, M.; Skoulika, S.; Aubry, A. *Mater. Res. Bull.* **1988**, *23*, 579−585.
(28) Hansson, E. *Acta Chem. Scand.* **1970**, *24*, 2969−2982.
(29) Nag, K.; Roy, A. *Thermochim. Acta* **1976**, *17*, 247−251.
(30) Usha, M. G.; Subba Rao, M.; Narayanan Kutty, T. R. *Thermochim. Acta* **1981**, *43*, 35−47.
(31) Bailar, J. C., Jr.; Jones, E. M.; Booth, H. S.; Grennert, M. *Inorg. Synth.* **1939**, *1*, 37.
(32) Kaziro, R.; Hambley, T. W.; Binstead, R. A.; Beattie, J. K. *Inorg. Chim. Acta* **1989**, *164*, 85−91.
(33) Wendlandt, W. W. *Anal. Chem.* **1958**, *30*, 58−61.
(34) van Niekerk, J. N.; Schoening, F. R. L. *Acta Crystallogr.* **1952**, *5*, 196−202.
(35) (a) Juríc, M.; Planinić, P.; Brničević, N.; Milić, D.; Matković-Čalogović, D.; Pajić, D.; Zadro, K. *Eur. J. Inorg. Chem.* **2006**, *2006*, 2701−2710. (b) Juríc, M.; Planinić, P.; Žilić, D.; Rakvin, B.; Prugovečki, B.; Matković-Čalogović, D. *J. Mol. Struct.* **2009**, *924−926*, 73−80.
(36) (a) Howe, A. T.; Shilton, M. G. *J. Solid State Chem.* **1980**, *34*, 149−155. (b) Bernard, L.; Fitch, A.; Wright, A. F.; Fender, B. E. F.; Howe, A. T. *Solid State Ionics* **1981**, *5*, 459−462.
(37) (a) Decurtins, S.; Schmalle, H. W.; Oswald, H. R.; Linden, A.; Ensling, J.; Gütlich, P.; Hauser, A. *Inorg. Chim. Acta* **1994**, *216*, 65−73. (b) Pellaux, R.; Schmalle, H. W.; Huber, R.; Fischer, P.; Hauss, T.; Ouladdiaf, B.; Decurtins, S. *Inorg. Chem.* **1997**, *36*, 2301−2308.
(38) (a) Clemente-León, M.; Coronado, E.; Galán-Mascarós, J. R.; Gómez-García, C. J. *Chem. Commun.* **1997**, 1727−1728. (b) Coronado, E.; Galán-Mascarós, J. R.; Gómez-García, C. J.; Martínez-Agudo, J. M. *Adv. Mater.* **1999**, *11*, 558−561. (c) Coronado, E.; Galán-Mascarós, J. R.; Gómez-García, C. J.; Ensling, J.; Gütlich, P. *Chem. - Eur. J.* **2000**, *6*, 552−563.
(39) Bénard, S.; Yu, P.; Audière, J. P.; Rivière, E.; Clément, R.; Guilhem, J.; Tchertanov, L.; Nakatani, K. *J. Am. Chem. Soc.* **2000**, *122*, 9444−9454.
(40) (a) Coronado, E.; Galán-Mascarós, J. R.; Gómez-Garcia, C. J.; Laukhin, V. *Nature* **2000**, *408*, 447−449. (b) Alberola, A.; Coronado, E.; Galán-Mascarós, J. R.; Giménez-Saiz, C.; Gómez-García, C. J. *J. Am. Chem. Soc.* **2003**, *125*, 10774−10775.
(41) Carling, S. G.; Mathoniere, C.; Day, P.; Malik, K. M. A.; Coles, S. J.; Hursthouse, M. B. *J. Chem. Soc., Dalton Trans.* **1996**, 1839−1843.
(42) Sanina, N. A.; Shilov, G. Y.; Ovanesyan, N. S.; Atovmyan, L. O. *Russ. Chem. Bull.* **1999**, *48*, 1581−1583.
(43) (a) Larionova, J.; Mombelli, B.; Sanchiz, J.; Kahn, O. *Inorg. Chem.* **1998**, *37*, 679−684. (b) Coronado, E.; Galán-Mascarós, J. R.; Gómez-Garcia, C. J.; Martinez-Agudo, J. M.; Martínez-Ferrero, E.; Waerenborgh, J. C.; Almeida, M. *J. Solid State Chem.* **2001**, *159*, 391−402.
(44) Jeong, N. C.; Samanta, B.; Lee, C. Y.; Farha, O. K.; Hupp, J. T. *J. Am. Chem. Soc.* **2012**, *134*, 51−54.
(45) (a) Slade, R. C. T.; Hardwick, A.; Dickens, P. G. *Solid State Ionics* **1983**, *9−10*, 1093−1098. (b) Howe, A. T.; Shilton, M. G. *J. Solid State Chem.* **1979**, *28*, 345−361.
(46) Kreuer, K. D.; Rabenau, A.; Weppner, W. *Angew. Chem., Int. Ed. Engl.* **1982**, *21*, 208−209.
(47) Wendlandt, W. W.; Simmons, E. L. *J. Inorg. Nucl. Chem.* **1965**, *27*, 2317−2323.
(48) Tanaka, N.; Nanjo, M. *Bull. Chem. Soc. Jpn.* **1967**, *40*, 330−333.
(49) Spees, T. S.; Sarma, C. A.; Fenerty, A. *J. Phys. Chem.* **1970**, *74*, 4598−4600.
(50) Usha, M. G.; Subba Rao, M.; Narayanan Kutty, T. R. *Thermochim. Acta* **1981**, *46*, 259−267.
(51) Sanina, N. A.; Shilov, G. Y.; Ovanesyan, N. S.; Atovmyan, L. O. *Russ. Chem. Bull.* **1999**, *48*, 1581−1583.
(52) Holmes, O. G.; McClure, D. S. *J. Chem. Phys.* **1957**, *26*, 1686−1694.
(53) For example: Mabbs, F. E.; Machin, D. J. *Magnetism and Transition Metal Complexes;* Chapman and Hall: London, U.K., 1973; pp 87−89.

DOI: 10.1021/acs.inorgchem.5b01176
Inorg. Chem. XXXX, XXX, XXX−XXX